IEEE Access
Multidisciplinary | Rapid Review | Open Access Journal

Received 22 November 2024, accepted 17 December 2024, date of publication 25 December 2024, date of current version 9 January 2025.

Digital Object Identifier 10.1109/ACCESS.2024.3522562

RESEARCH ARTICLE

SafeRespirator: Comprehensive Database for N95 Filtering Facepiece Respirator Leakage Detection Including Infrared, RGB Videos, and Quantitative Fit Testing

GEOFFREY MARCHAIS[1], MOHAMED ARBANE[1], (Graduate Student Member, IEEE), BARTHELEMY TOPILKO[1], JEAN BROUSSEAU[1], CLOTHILDE BROCHOT[1,2], YACINE YADDADEN[1], ALI BAHLOUL[1,2], AND XAVIER MALDAGUE[3], (Life Senior Member, IEEE)

[1]Department of Mathematics, Computer Science, and Engineering, University of Quebec at Rimouski, Rimouski, QC G5L 3A1, Canada
[2]Institut de Recherche Robert-Sauvé en Santé et en Sécurité du Travail (IRSST), Montreal, QC H3A 3C2, Canada
[3]Department of Electrical and Computer Engineering, Laval University, Quebec City, QC G1V 0A6, Canada

Corresponding author: Geoffrey Marchais (geoffrey.marchais@uqar.ca)

This work was supported in part by the "Filtering Facepiece Respirator (FFR) Protective Devices—Development of an Easy-to-Use Method to Detect Leak and Assess Face Seal Tightness Using Infrared (IR) Imaging" Project which Institut de Recherche Robert-Sauvé en Santé et en Sécurité du Travail (IRSST) and Mitacs Fund under Grant IRSST 2022-0008, and in part by Mitacs under Grant IT37899.

This work involved human subjects or animals in its research. Approval of all ethical and experimental procedures and protocols was granted by the University of Quebec at Rimouski (UQAR) and Laval University Research Ethics Committees under Approval No. 2024-276. Date of Award: September 26, 2023.

ABSTRACT The COVID-19 pandemic underscored the challenges of performing mandatory Quantitative Fit Tests (QNFT) for healthcare professionals and the limitations of self-administered fit checks. To address this, it is crucial to develop faster and more efficient methods for detecting, locating, and quantifying Filtering Facepiece Respirators (FFRs) leakage, providing wearers with immediate feedback on their safety. Infrared (IR) technology, which relies on temperature variation analysis around the face seal, has proven effective for locating leakage but has not yet achieved automated quantification. This paper introduces a validated protocol for creating a comprehensive database to advance automatic leakage detection. The database includes synchronized and calibrated IR and RGB video data, along with QNFT results, collected from 62 participants wearing four different N95 FFR models in four distinct positions. High-performance IR and RGB cameras were used to precisely capture temperature variations, while a PortaCount® instrument served as the reference for fit quantification. Preliminary results using the MediaPipe approach with synchronized and calibrated RGB and IR videos demonstrate that precise tracking of the human face is achievable even with an FFR. The normalized cross-correlation methods further highlight the capability of IR imaging to accurately monitor and detect leakage. This breakthrough paves the way for real-time, automated detection of N95 FFR leakage, potentially deployable at operator workstations. This large, high-quality, open-access database is available to the scientific community to drive innovation in respiratory protection research and beyond.

INDEX TERMS Database, infrared imaging, N95 FFR leakage, occupational health and safety, quantitative fit testing, BigData.

I. INTRODUCTION

A N95 Filtering Facepiece Respirator (N95 FFR) is a device that protect the wearer from inhaling harmful aerosols.

The associate editor coordinating the review of this manuscript and approving it for publication was Nuno M. Garcia.

However, only N95 FFR devices correctly adapted to the wearer's face can offer adequate protection. For N95 FFR, which are the most frequently used in healthcare [1], the biggest contributory factor to the loss of protection is a leakage through the face seal [2], [3]. This implies that the protection offered by an FFR is significantly affected by the impaired fit between the FFR and the face [4]. FFR fit can be determined by qualitative or quantitative methods [5]: Quantitative Fit Test (QNFT) or Qualitative Fit Test (QLFT). These methods enable to choose the N95 FFR best suited to the wearer's facial morphology. Once the N95 FFR has been selected, the wearer must perform a self-test named fit check or user-seal-check each time it is used. This test checks the tightness of the N95 FFR through positive and negative pressure tests.

Concerning QNFT and QLFT, these methods enable the choice of the best-suited N95 FFR to the wearer's facial morphology. The distinction between QLFT and QNFT lies in both the method and the Pass/Fail criteria. In QLFT, the tester must verify the subject's ability to detect the challenge agent (sensitivity test) during breathing exercises. The subject must indicate if he detects the challenge agent during the QLFT; it is deemed ''Pass'' when the challenge agent is not detected. Conversely, QNFT employs a particle counter to calculate a fit factor. To obtain a test labeled ''Pass'', it requires a minimum fit factor of 100 for half facepieces [5]. However, these different methods have shown some limits. Indeed, they do not enable the precise leakage localizations, which are detected solely through irritation or a low fit factor. Additionally, they offer neither a visual representation of leakage nor an accurate measurement of their severity. Furthermore, these tests are not automated, requiring supervision by a specially trained professional. Taken together, fit testing is both resource-intensive and expensive in terms of time and cost [6].

Concerning the fit check, before COVID-19, Huh et al. [7] have already studied the accuracy of this fit check and have shown that almost 50% of N95 wearers don't perform an adequate verification. Lam et al. [8] and Regli et al. [6] have both concluded that the user-seal-check has low sensitivity, accuracy, and predictive value in determining the fit of N95 FFR. It is unreliable in detecting a proper fit or identifying leakage. Furthermore, many healthcare workers have been extensively exposed to COVID-19, and a significant proportion of them have contracted the virus [9], [10]. Furthermore, both this fit check and the QLFT rely on the judgment of each participant [6], meaning their results from these tests depend on the judgment of each participant.

All things considered, it seems important to find alternative methods to conventional fit testing and fit checking. These methods should enable the detection of N95 FFR leakage, specifically by locating and quantifying leakage automatically, to reduce costs and save time. Infrared (IR) technology has already demonstrated its capacity to detect leakage. Indeed, studying temperature variations at the face seal can help identify FFR leakage. These temperature changes arise from the contrast between the ambient air (the inhaled air) and the warm exhaled air [11].

Some studies have investigated leakage detection on N95 FFR using IR imaging [4], [12]. These studies have shown that IR imaging can assess whether an FFR is properly worn and can have a complementary role in QNFT. Harber et al. [13] have also shown that there is a correlation between FF and IR Imaging, but it was insufficiently strong to substitute for QNFT.

Other studies have focused on the integration of deep learning models for N95 FFR leakage detection using IR imaging [14], [15], [16]. All these studies have shown the potential of artificial intelligence in detecting air leakage for FFR wearers. Characteristics of the database used for their study and their model's training are given in the comparison Table. 1. Each study has collected IR images of human subjects wearing N95 FFR and has also conducted a fit test (QNFT or QLFT) [14], [15], [16].

Several limitations of their databases are mentioned in their respective studies. Indeed, Chapman et al. [14] have used only one type of P2 FFR, the flat-fold FFR, and have observed temperature changes solely in the nose area when studying the temperature gradient on the FFR.

Bari et al. [16] have identified immobilization of the participant as the biggest challenge in IR image recording. They have concluded that human movements influence image processing and results.

Similarly, Siah et al. [15] have faced several limitations, including a small sample size, an imbalance between male and female participants, and the use of only one type of N95 FFR, just like Chapman et al. [14]. Additionally, the study by Siah et al. [15] has lacked a FF for each test, as all participants have failed the QLFT, and there are no IR images of participants wearing an FFR after a 'Pass' QLFT test.

In summary, these databases appear to be insufficient for training deep learning models designed to automatically detect and quantify leakage around the face seal of a moving participant. Several critical gaps persist within these datasets: the absence of four different viewpoints recorded, the lack of FF measurements for each test, a limited and imbalanced number of participants, a large volume of data primarily consisting of IR videos, the use of different FFR N95 and finally the absence of methods to account for participant motion [14], [15], [16].

Considering the context and the various limitations highlighted in previous studies, the objective of the present study is to develop a comprehensive and robust database that adheres to several key criteria:

→ Collect data on a large and balanced number of participants;
→ Include participants with diverse facial morphologies wearing different types of N95 FFR;
→ Record high-definition IR and RGB videos from multiple angles of participants wearing N95 FFR;

→ Conduct two QNFT for each N95 worn by a participant, one at the beginning and one at the end of the test;
→ Make the database accessible to the scientific community.

The addition of RGB video recording enables the tracking of various points on the face of a moving person wearing an N95. For instance, Jiang et al. [17] have used RGB and IR sensors to detect respiratory infections by first identifying face and N95 FFR regions in the RGB frames, then mapping these regions to the thermal frames, and finally capturing the regions of interest (ROIs) in the thermal frames. Some computer codes such as MediaPipe [18] enable human face tracking on RGB videos, which will eliminate the problem of movements, as quoted by Bari et al. [16]. The version of MediaPipe that can create landmarks on the face can't work on IR images due to the nature of IR videos and because the MediaPipe face mesh was trained on RGB visual datasets. The MediaPipe Face Mesh is based on deep learning, utilizing a convolutional neural network (CNN) to detect and track facial landmarks accurately in real-time. This is primarily because IR technology captures thermal radiation, which significantly differs from the visual light spectrum in RGB images. In addition, IR and RGB data can be merged for face tracking in IR videos. Numerous studies have explored this fusion using RGB and IR cameras [19], [20], as well as methods to calibrate these cameras with a checkerboard [21], [22].

II. METHODOLOGY

A. MATERIAL

1) IMAGING SYSTEM CONFIGURATION

The study aims to investigate temperature variations of a human face wearing an N95 FFR during normal breathing, considering human movement. For that, a complete imaging system was developed to study these variations, including four different elements: an RGB camera, an IR camera, a synchronization system and a Stereo camera calibration system [23]. The two cameras used, are detailed in Table. 2. They were chosen for their high-resolution level and frame rate similarity. A 50 mm lens was chosen to operate with the IR camera because this lens enables a display similar to that of the RGB camera.

The imaging system was developed on the CAO software, SolidWorks 2022 (Dassault Systems, Waltham, MA) and was printed with the Ultimaker S5 3D Printer (Ultimaker B.V., Utrecht, Netherlands) as shown in black in the Fig. 1.

A RGB camera deep adjustment was added to this system for a better alignment between the two lenses. The main requirement of this imaging system was the necessity to create a system where the lenses of the cameras were as close as possible to minimize the distance between these lenses [21]. Indeed, it enables the recording of similar videos and facilitates calibration between these two cameras. Another requirement was that each camera should not move relative to the other during all data collection to avoid a remaking of calibration.

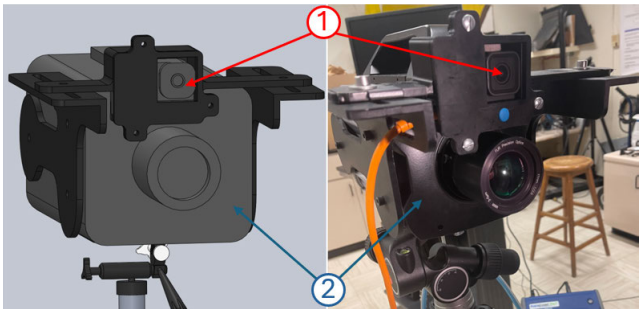

FIGURE 1. Modeling and design of the imaging system, 1) RGB camera, 2) IR camera.

2) IMAGING SYSTEM CALIBRATION

Once the cameras were installed, immobile and ready for use, they needed to be calibrated. Stereo camera system calibration involves aligning two cameras to capture the same scene accurately and reconstructing it in 3D, using a known pattern like an 8×8 checkerboard to determine intrinsic and extrinsic parameters. The calibration used an aluminum checkerboard, made by sticking adhesive vinyl on an aluminum sheet, with the checkerboard pattern cut into the vinyl. Aluminum's low emissivity ($\approx$0.02 at 20°C [24]) contrasts with vinyl's high emissivity ($\approx$0.95 at 20°C [25]), allowing an IR camera to capture the difference when a lamp heats the checkerboard. The process starts by capturing multiple images of the checkerboard from different angles to calculate intrinsic parameters like focal length and optical center and then estimating extrinsic parameters such as relative position and orientation. Using about 10 pairs of IR and RGB images of the checkerboard in different positions enhances accuracy (Fig. 2). Regular recalibration is recommended to account for changes in camera positions, lens focus, and ambient conditions, ensuring optimal 2D correspondences and precise 3D reconstruction for high-precision 3D imaging [26]. Ten pairs of images were captured daily for calibration during each day of data collection.

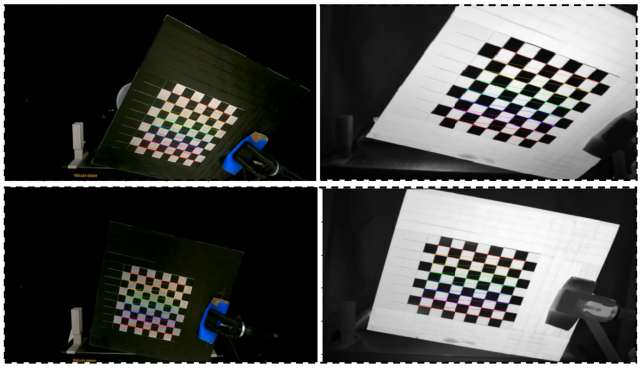

FIGURE 2. Two IR and RGB image pairs of the aluminum checkerboard in 2 different positions for calibration.

TABLE 1. Information about database used to develop their deep learning models.

Studies	Chapman et al. [14]	Bari et al. [16]	Siah et al. [15]
Participants (Female/Male)	48 (36/12)	8 (2/6)	17 (15/2)
Fit Test Type	QNFT	QNFT	QLFT
Fit Test Device	TSI Portacount Model 8048	TSI Portacount Model 8038	N/A
IR Camera Model	FLIR One Gen3 - iOS	Jenoptik VarioCam®	FLIR T365
IR Camera Resolution	160*120 pixels	640*480 pixels	320*240 pixels
Points of View recorded	(1) front	(5) top, left, bottom, front, right	(5) top, left, bottom, front, right
IR data used	48 images	462 images	N/A

TABLE 2. Characteristics of two cameras used to collect data.

Cameras	RGB	IR
Manufacturer	GoPro Inc.	FLIR Systems
Model	Hero 9	X8501sc
Resolution	1920*1080 pixels	1280*1024 pixels
Sensitivity	∅	<20 mK
Frame Rate	30 Hz	(25 to 30)[a] Hz
Software used	OBS Studio	ResearchIR Max

[a]Frame rate for the IR camera was no constant, varying from 25 Hz to 30 Hz. However, the duration of each IR video was constant in this study (35 seconds).

3) IMAGING SYSTEM SYNCHRONIZATION

Once IR and RGB cameras were fixed and calibrated, it was important to synchronize the recordings from each camera to avoid a time difference between IR and RGB videos. The two cameras work with different software, each with a different time delay at the start of recording, making automatic synchronization complicated. A synchronization system was developed to solve this issue, controlled by Bluetooth and composed of a halogen lamp, an electromagnet, an Arduino Uno and 3D printing pieces. This system was placed just behind the participant on a wood panel. For each video recording start, a 10-second delay allowed the lamp to heat up. At the end of this period, a pulse of heat and light was visible to the two cameras, as shown in Fig. 3. Furthermore, a computer code was developed to recognize this pulse and synchronize the IR and RGB videos.

FIGURE 3. Two IR and RGB image pairs with and without pulse of heat and light (encircled in red) for synchronization.

4) QUANTITATIVE FIT TESTING

To detect an N95 FFR leakage with IR technology, it was essential to rely on a technology that is already used daily by professionals and has already proven its efficiency. The reference instrument that was used in this study is the PortaCount® Instrument, Model 8038 (TSI Incorporated, Shoreview, Minnesota, USA). It enables the performance of a QNFT by counting particles inside and outside the N95 FFR during 8 breathing exercises, as described by OSHA. The Fit Factor (FF) is then calculated by dividing the number of particles outside the N95 FFR by the number of particles inside. The PortaCount® Model 8038 measures FF from 0 to 200. For an N95 FFR, the success criterion to pass a QNFT is an FF higher than 100 [5]. The instrument must be used in a controlled environment with enough particles in the ambient air. For that, a particle generator, the 24 Jet Collision Nebulizer (BGI, Inc) was used. It operates with different pressures and solutions, but in the context of the present data collection, a pressure of 30 PSI and a salt solution ($c = 0{,}05$ g/mL) were chosen. These parameters enabled constant particle generation around 10000 particles/cm^3 in ambient air and were safe for participants' health. The average diameter of the generated particles was less than 100 nanometers.

5) OVERALL INSTALLATION

The installation integrated the various instruments and allowed one participant to sit in front of the cameras. As shown in Fig. 4, it consisted of a dark tent, a swivel chair and the imaging system. The dark tent served two purposes. It minimized reflectivity and prevented external disturbances during data collection and calibration on the checkerboard, as done by Roberge et al. [4]. The dark tent also created a smooth bottom on videos, making the synchronization easier. The swivel chair allowed participants to rotate with the chair instead of turning their heads, thus limiting their head movements. Indeed, head movements can change N95 FFR fit and by the same way affect correlation between FF and IR evaluation. The tripod of the imaging system and the swivel

chair were fixed to the ground. This helped to maintain a constant distance of 50 centimeters between the participant's face and the camera lenses. Keeping this distance constant helped reduce the need for frequent adjustments of the IR camera lens and, consequently, minimized the number of camera calibrations required.

This setup was implemented in a laboratory with controlled temperature and relative humidity, maintained using a thermostat set to 21°C. During data collection, the temperature ranged from 20°C to 22.5°C, while the relative humidity fluctuated between 17% and 23%.

FIGURE 4. Final installation including the imaging system, the PortaCount®, the dark tent and the swivel chair.

B. METHODS

1) PARTICIPANTS

The ethical approvals to conduct the data collection on participants were obtained by the University of Quebec at Rimouski (UQAR) and Laval University Research Ethics Committees (approval number 2024-276) in the fall of 2023. Participant recruitment was done in the student community of Laval University. To be recruited, the participant had to meet the following eligibility criteria, similar to those for a QNFT [5]: Not show flu-like symptoms, not have skin irritation or inflammation on the face, not have eaten, drunk, or smoked 1 hour before the event, for men, be clean-shaven at least 24 hours beforehand. 62 participants participated, 36 women (58%) and 26 men (42%). Before starting data collection, each one signed two consent papers, one to participate in the data collection and another to give agreement for image sharing in publications or reports. Refusing to share their data did not result in the cancellation of data collection.

TABLE 3. N95 FFR characteristics tested during data collection.

Manufacturer	N95 Type	Valve	Size	Test Count
3M	8210	No	Standard	62
3M	8210V	Yes	Standard	12
3M	VFlex 9105	No	Standard	27
Moldex	2200	No	M/L	62
Moldex	2300	Yes	M/L	12
Honeywell	DC300	No	One Fit	61
Honeywell	DC300V	Yes	One Fit	12

Each N95 FFR are Molded Cup shaped, except 3M VFlex 9105, which is a V-shaped pleat. Total tests conducted = 248

2) PROTOCOL

After the consent papers were signed and following an explanation of the protocol for data collection, the data collection process began. Each participant tested 4 different N95 FFR out of 7 available options (Table. 3).

The N95 FFRs from various manufacturers were selected for their distinct geometries, designed to create diverse leakage scenarios. Indeed, one of the objectives of this study is to examine different leakage scenarios occurring at various locations around the face seal. One can reach this objective by multiplying N95 FFR geometries and participant facial morphologies. It is important to notice that the data collection was not performed to test the N95 FFR's performance to fit. The participants did not receive instructions about wearing an N95 FFR. Therefore, the participants unintentionally created leakage.

As illustrated in Fig. 5, participants followed a test sequence that involved setting up an N95 FFR, undergoing an initial QNFT, breathing in front of the imaging system, and finally, completing a second QNFT. This protocol was developed following a preliminary study on a Static Advanced Headform wearing an N95 FFR. This study helped establish the number of fit tests conducted and the number of views recorded.

Data collection operated in the following sequence. First, participants, seated in front of the cameras, were given two minutes to put on and adjust an N95 FFR. QNFT tests were carried out at the beginning and end of the collection. It consisted of three exercises: normal breathing (50 seconds), deep breathing (50 seconds), and normal breathing (50 seconds). The two QNFT allowed verification that the N95 FFR fit did not change during the collection. The difference X (with $X = FF1 - FF2$) and the average between these two FF were then calculated. The difference enabled to class the reliability of each test. The greater difference, the less reliable the data. Indeed, a large difference meant the N95 FFR fit had changed during test. On the other hand, the average gave a global FF of the test.

The aim of the database is to correlate FF with IR videos, so 3 exercises were selected to observe the same leakage during the IR test. Exercises and sample time were selected from the eight exercises outlined in the OSHA protocol, as they are less likely to modify the face seal during testing.

During the IR test, the subject breathed normally and assumed four different positions over 35 seconds, positioning their face in front of the cameras, upwards, to the left,

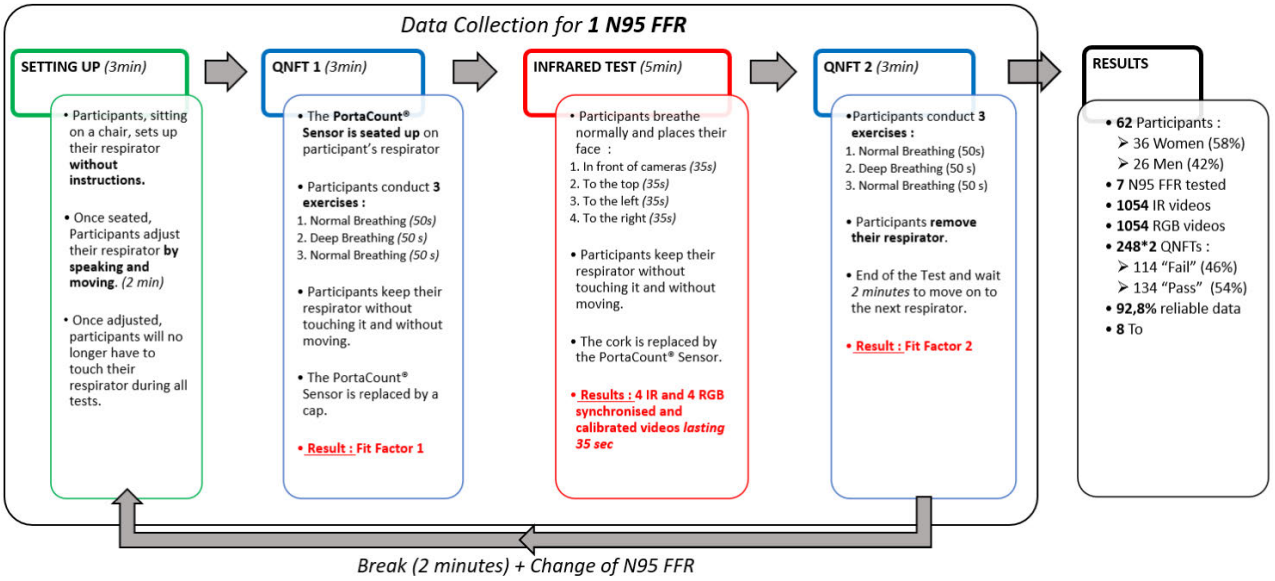

FIGURE 5. Detailed data collection protocol for 1 N95 FFR tested.

and finally to the right. These positions enabled to capture exactly and totally the participant face seal. Indeed, with one view, for example in front of cameras, the IR camera can't capture the entire face seal. To take these positions, the participants used the swivel rotation to avoid breaking the face seal and not changing their N95 FFR fit. It was requested that the participants minimize their head movements. The sweating of these participants was not controlled. Between each QNFT and the IR test, a replacement between a cap and the PortaCount® sensor was done. It was enabled to capture IR videos without the PortaCount® sensor influencing temperature variations on the N95 FFR or the face seal in IR videos. A cap was used because a QNFT requires the N95 FFR to be perforated to accommodate the PortaCount® sensor. Time recording was chosen to capture enough breathing cycle to study them. For a normal human breathing, frequency breathing is comprised between 12 and 20 cycles per minutes [27]. So, a time recording equal to 35 seconds represents several cycles captured between 7 and 12 cycles. At the end of each N95 FFR (starting from the 11th participant) a question about a possible feeling of leakage was asked to the participant. Their answer enables cross-reference information between an IR video, an FF and a participant's feelings. This information makes it easier to locate leakage with certainty.

Between each N95 FFR, the participant had a break of 2 minutes to breathe normally without N95 FFR. When the participant's face temperature was back to normal at the end of data collection, a last IR and RGB video recording of the participants without wearing an N95 FFR was done. This last recording enabled the evaluation of the size of the participant's face with an algorithm which calculates the number of pixels compared to a known face reference. Face length and face width of each participant were measured, and so it enabled the placement of each participant in the bivariate NIOSH Panel (Fig. 6). This figure shows the diversity of participant facial morphologies in this data collection, which is one of the aims of this study.

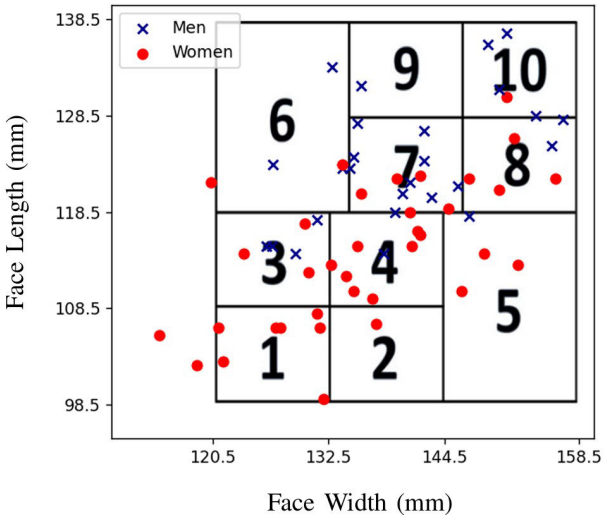

FIGURE 6. NIOSH bivariate panel as determined by Zhuang et al. [28] and distribution of 62 participants' face length and width.

III. RESULTS

A. RECORDING VISUALIZATIONS

As described previously, for each participant and each N95 FFR, IR and RGB videos lasting 35 seconds were captured in four different positions as shown in Fig. 7. OBStudio Software [29] (OBStudio, Inc.) enables the recording and export of RGB video in.mp4 format, while ResearchIR Max [30](FLIR Systems, Inc., Wilsonville, Oregon, USA) records in.ats format, a proprietary FLIR format that is

TABLE 4. Test reliability classification according to the difference between FF1 and FF2.

Reliability	Difference X	Test Count	Percentage(%)
Very reliable	$0 \leq X \leq 25$	212	85,5
Reliable	$25 < X \leq 50$	18	7,3
Little reliable	$50 < X \leq 100$	14	5,6
Unreliable	$100 < X \leq 200+$	4	1,6
Total	$0 \leq X \leq 200+$	248	100

unusable without Research IR Max and so in algorithms. The.tiff format, known for its high-quality images, was finally used to export these videos to avoid information and quality loss. For each participant, 34 videos were recorded, 17 IR videos (.tiff and.ats) and 17 RGB videos (.mp4). 4 positions for each of 4 N95 FFR = 16 videos + 1 video without an N95 FFR. As mentioned before, the four positions allow visualization of the face seal entirely. Additionally, the IR camera's high sensitivity and high acquisition frame rate allow for precise monitoring of temperature variations around the face seal, with a sensitivity of less than 20 mK.

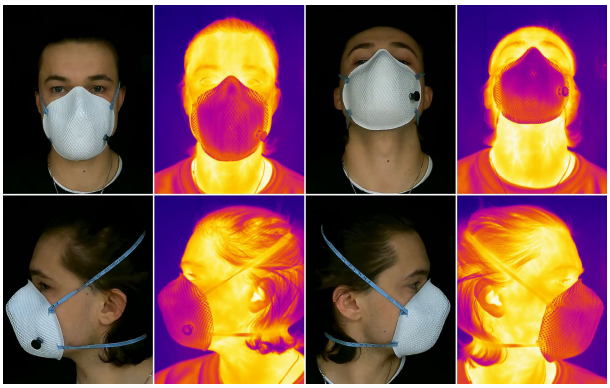

FIGURE 7. Visualization of IR and RGB images in 4 different positions: front, top, left, right.

B. TEST RELIABILITY

In addition to IR and RGB videos, each N95 FFR tested by a participant involved two QNFT, resulting in two measured fit factors. The difference and the average of the fit factors were calculated to classify each test. The difference $|FF1 - FF2|$ was used to classify the reliability of a test, as shown in the Table. 4. There were, in totality, 62 participants, and each one wore 4 N95 FFR, so there were 248 (62*4) tests. This classification was decided according to the accuracy of PortaCount® which is ±20 when the higher fit factor measurable is 200 [31]. With this classification, more than 92.8% of data collected are considered as reliable or very reliable. A difference between FF1 and FF2 greater than 100 indicates that the N95 FFR fit changed significantly during data collection. This classification helps determine which data will be used first and which will be discarded.

C. TEST CLASSIFICATION

Regarding the average between FF1 and FF2, this value was used to classify each test according to the FF. A distribution of the number of QNFT based on FF is presented in Fig. 8. This distribution can also be used to count how many tests are classified as 'Pass' and 'Fail.' A test is considered a 'Pass' if its FF is higher than 100 [5]. In these tests, 114 (46%) are considered as "Fail" and 134 (54%) as "Pass". The database is then constituted for each test by the bivariate parameter of the participant, 17 IR videos, 17 RGB videos, 2 FF labels and a test reliability.

TABLE 5. Example of 2 tests for 2 participants.

Participant N°	N95 Type	Fit Factor	Leakage Area Feeling[a]
60	3M 8210	10.5	Left Nose
41	3M 8210	200+	No Feeling

[a]The point of view on the leakage area feeling is always provided by the data tester, namely the observer.

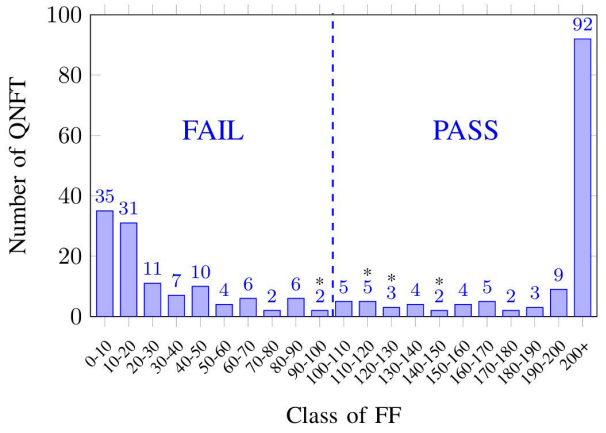

FIGURE 8. Test distribution according to the average between FF1 and FF2 (*Corresponds to the class of FF with 1 unreliable test).

D. PRELIMINARY RESULTS

To show an example of using this database, sequences from two different participants, were processed and compared. The sequences from participants number 60 and 41 are used as an example. The information regarding these tests is detailed in Table. 5.

For each participant and each recorded point of view, it is possible to visualize the temperature variations between exhalation and inhalation over a single breathing period. These variations are calculated as the pixel-wise subtraction between two images corresponding to the peak temperature of the exhalation and the inhalation: $I_{exhalation}$ and $I_{inhalation}$:

$$I(i,j) = I_{\text{exhalation}}(i,j) - I_{\text{inhalation}}(i,j), \tag{1}$$

where i and j represent the pixel coordinates, with $i \in [0, 1280]$ and $j \in [0, 1024]$. Fig. 9 presents these temperature variations for one single breathing period. These heatmaps align with the leakage feeling reported by participant 60 in the area of the left nostril and the absence of such a feeling reported by participant 41. This presence and absence of leakage are also consistent with the FF measurements collected for these two participants wearing a 3M 8210 N95 (Table 5).

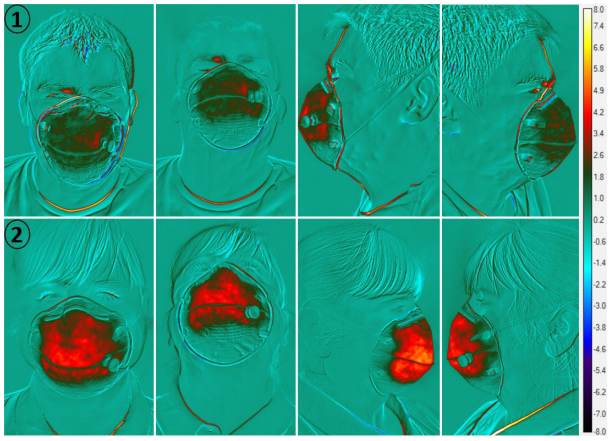

FIGURE 9. Variation of temperature (in °C) over a single breathing period for each recorded point of view. 1) Participant 60, 2) Participant 41.

However, this subtraction method has its limitations, which are evident in the heatmaps (Fig. 9). Specifically, some temperature variations are not due to leakage. For instance, temperature variations of approximately 7-8°C are observed near each participant's collar. This phenomenon is also evident for participant 60, particularly around the face seal and near the right ear in the "front" view, as well as at the forehead level in the "right" view ((1) in Fig. 9). These temperature variations are caused by movement and can be attributed to the temperature difference between the pullover and the skin in the collar area. Even though these two participants exhibit only slight movements, small movements can lead to errors in temperature readings. Overall, accounting for participant movement is crucial for accurate leakage detection, a finding consistent with the study conducted by Bari et al. [16].

The method used to account for human movements in this study is the MediaPipe [18] approach, which utilizes both RGB and IR videos. Specifically, the MediaPipe method enables the tracking of key points on a moving human face in RGB videos. After synchronizing the RGB and IR 3, stereo camera system calibration is applied [21], [22] using the checkerboard shown in Figure 2. MediaPipe is applied on the RGB images, as shown in Fig. 10 (left side). The information is then transferred to the IR sequence, where the landmarks of the face mesh detected by MediaPipe are mapped onto the IR images, as illustrated in Fig. 10 (right side). This process ensures accurate correspondence between the RGB and IR data, enabling robust facial feature detection across both modalities.

After identifying the landmarks, it is possible to extract the temperature at specific points on the face (Fig. 10). In this case, landmarks numbers 56 and 464 are used. The results of the temperature measurements at these points are shown in Fig. 11. This approach enables precise thermal analysis of the face with a sensitivity of less than 20 mK, based on accurately mapped landmarks from RGB images, even when the participant moves during the recording.

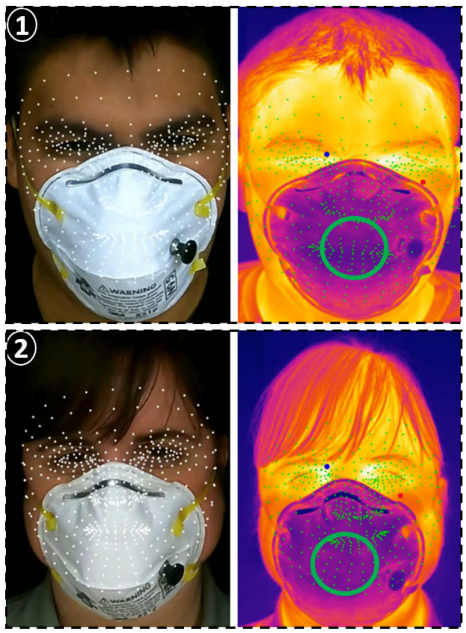

FIGURE 10. Application of MediaPipe on RGB/IR Images after synchronization and calibration. 1) Participant 60, 2) Participant 41. Landmark 56: blue point on the left side, at eye level; Landmark 464: red point on the right side, at cheek level; Center of mask: green circle. The size of the landmarks is enlarged for better visibility; their original size is 4*4 pixels.

After extracting the landmarks on the IR images, landmarks that could potentially indicate thermal leakage were selected. This selection allows visualizing the temperature at these critical points. Fig. 10 shows the locations of these selected landmarks ((blue point for landmark 56 on the left side, at eye level, and red point for landmark 464 on the right side, at cheek level). Fig. 11 presents a diagram of the temperature changes over time at these two points for participants 60 and 41. This analysis helps in understanding the thermal behavior of the face at specific landmarks under different conditions.

This diagram is consistent with the heatmaps (Fig. 9). It's also noticeable that the mean temperature fluctuates over the recording period depending on the landmark. Landmark 56 registers a higher mean temperature compared to landmark 464. For the same landmark, this mean temperature also varies between participants. As for temperature fluctuations, they are not constant throughout the test, as illustrated by the blue curve for participant 60. The preliminary results, therefore, show that the method is capable of showing the presence of potential leakage.

It is also valuable to analyze the temperature evolution of the N95 FFR, as it provides essential insights into each participant's breathing patterns, including respiratory rate and amplitude. However, detecting the center of the mask to calculate the respiratory temperature was challenging, while the mask was not part of the face. To address this issue, a semantic segmentation method was implemented using a U-Net variant proposed by Arbane et al. [32]. This deep

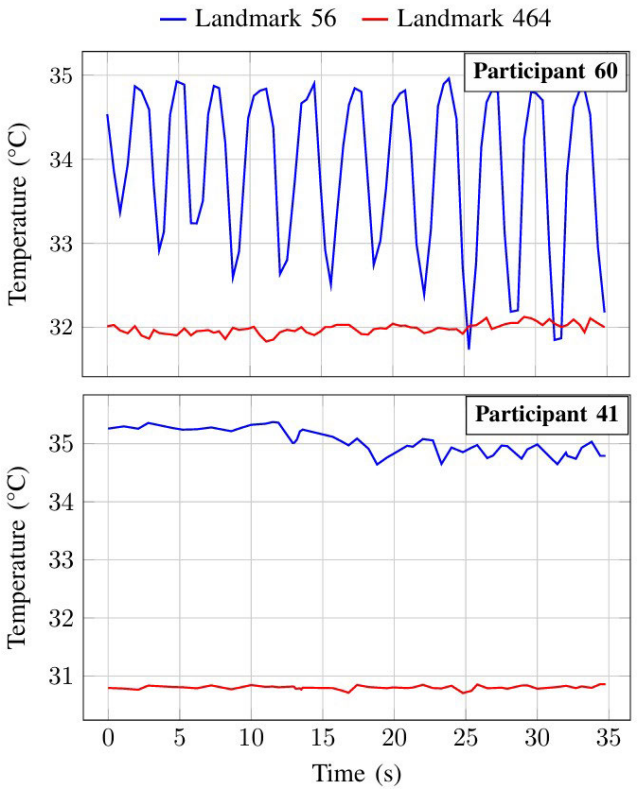

FIGURE 11. Comparative analysis of temperature variations between two participants at identical landmarks.

learning model enables the automation of N95 FFR detection and was developed on human subjects wearing N95 FFR. After segmentation, the center of the mask (in green in Fig. 10) was selected to measure the breathing pattern and temperature variations, including frequency and amplitude. Fig. 12 presents the two participants' average temperature evolution on the N95 FFR. Additionally, a spectral analysis could be performed to identify the dominant frequency components.

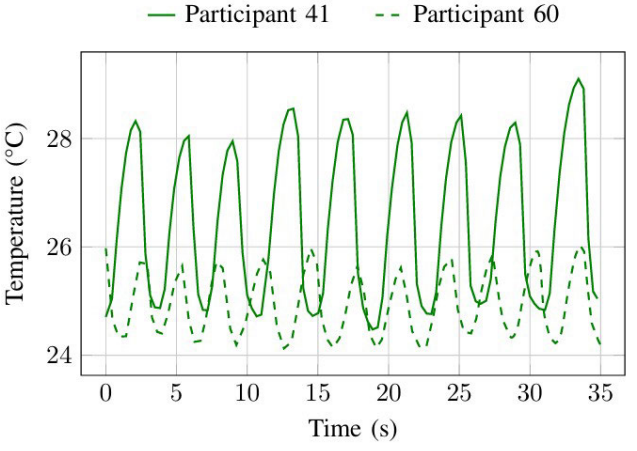

FIGURE 12. Evolution of the average temperature across all pixels within the green circle at the center of the N95 FFR, using mask segmentation [32].

To determine whether temperature variations are due to a leakage rather than movements, blinking, or external factors, one approach is to analyze the similarity between thermal signals recorded at the N95 FFR (Fig.12) and at the leakage site (Fig.11) for each participant. This can be achieved using normalized cross-correlation [33], which measures the similarity between two signals with a time lag (τ). This method disregards the continuous component and the signal amplitudes, focusing solely on temperature variations, which are indicative of leakage [11]. A high correlation value (close to 1) indicates a strong similarity between these thermal signals and suggests the presence of a potential leakage. Indeed, the breathing pattern will be more pronounced in areas with leakage than in those without.

These two thermal signals are discrete and sampled at a frame rate of 30 Hz over a duration of 35 seconds, resulting in N (the number of samples) being 1050. Formulas (2) enables to normalize a discrete signal $g[k]$ with μ_g the mean and σ_g the standard deviation of the discrete signal.

$$g_{\text{norm}}[k] = \frac{g[k]-\mu_g}{\sigma_g}, \text{ where :}$$
$$\mu_g = \frac{1}{N}\sum_{k=1}^{N} g[k] \;\; ; \;\; \sigma_g = \sqrt{\frac{1}{N}\sum_{k=1}^{N}\left(g[k]-\mu_g\right)^2} \quad (2)$$

The normalized cross-correlation $R_{gf}^{\text{norm}}[n]$ between two discrete signals $g[k]$ and $f[k]$, where n represents the sample lag and $*$ denotes the convolution product, is defined by formula (3).

$$R_{gf}^{\text{norm}}[n] = (f_{\text{norm}} * g_{\text{norm}})[n]$$
$$R_{gf}^{\text{norm}}[n] = \sum_{k=0}^{N-1} f_{\text{norm}}[k]\cdot g_{\text{norm}}[k+n] \quad (3)$$

Once calculated, this normalized cross-correlation can be expressed as a function of the time delay τ using the frame rate. Fig. 13 presents the normalized cross-correlation R for two studied landmarks (56 & 464) with the thermal signal at the N95 FFR for each participant as a function of the time lag (τ). A strong correlation is observed for landmark 56 of participant 60, reaching 0.91 at a time lag of 0.26 seconds ($R(0.26) = 0.91$, the black cross on Fig. 13). This strong correlation supports the potential leakage detected in Fig. 11. In contrast, for the other landmarks, the correlation is significantly lower, falling below 0.35.

The calculation of the normalized cross-correlation at each Mediapipe landmark with the thermal signal at the FFR could allow for precise leakage detection. Other methods to check the similarity between two signals, such as cross-spectral analysis [34] or Pearson correlation [35], could also be explored. Future work will investigate these methods and determine which is most suitable for detecting N95 leakage. Additionally, future efforts will focus on developing a method to quantify each leakage by analyzing the thermal signal amplitude at specific landmarks around the face seal. These

methods will be applied to the entire dataset, facilitating the efficient training of deep learning models.

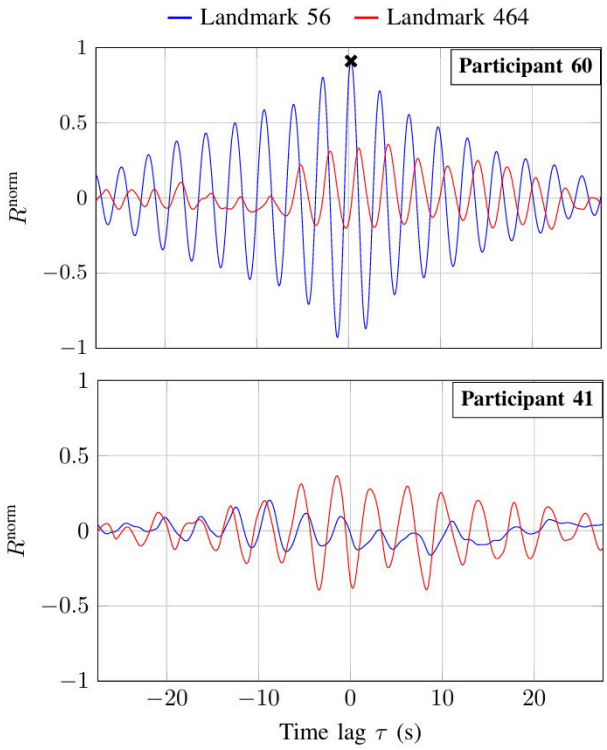

FIGURE 13. Normalized cross-correlation R^{norm} between breathing pattern and each studied landmark (56 & 464) for two participants (60 & 41).

More recently, Arbane et al. employed their semantic segmentation approach [32] for a purpose different from that of this study. They used it to eliminate the need for RGB videos by applying their model to each frame, enabling the detection of FFR and the face seal at each position of a participant. This allows for the study of the face seal independently of the participant's movements.

IV. DISCUSSION

The development of the testing installation has allowed for the collection and compilation of a database of participants wearing N95 FFR in various positions. Preliminary results demonstrate the method's capacity to detect potential leakage. Concerning the reliability of data collected, based on the difference between FF1 and FF2, 85.5% of the data are considered very reliable, 7.3% are considered reliable, 5.6% are considered little reliable and 1.6% are considered unreliable. The unreliable data is explained by change in the FFR fit during the recording of IR and RGB videos. These videos are still usable, but the labeling of the FF on these tests remains unreliable.

Recording videos to accurately capture the face seal proved complex during data collection. Positioning the participant with meticulous precision is imperative to obtain appropriate data. Excessive rotation of the chair results in partial capture of the face seal. Using four views of the participant's face ensured capturing the entire face seal. However, achieving adequate capture might require fewer views.

The objective is not only to locate leakage, but also to quantify it. Labeling each test using the FF will allow leakage-level classes to be created. Currently, the two main existing classes are "Pass" and "Fail", for the two fit testing methods: QNFT and QLFT. However, given the distribution of PortaCount® measures (Fig. 8), there is potential for refining and multiplying these classes.

This database could be also used to detect respiratory issues by studying breathing patterns through the mask, assessing the thermal impact of wearing an N95 FFR, or studying the fluid mechanics of breathing through an N95 FFR. For example, Arbane et al. [32] have already utilized these data to develop a deep learning model aimed at improving the segmentation of an N95 FFR using IR videos. This model demonstrates high accuracy and enables precise analysis of the face seal. Future work will focus on an in-depth investigation of the face seal to enable automatic leakage detection, alongside exploring alternative correlation methods proven to enhance this process. Statistical analyses will be employed to determine the most effective approach. Making this localization and quantification automatic would also allow detecting leakage at workstations close to the operators, ensuring them respiratory protection throughout their activity. Many other fields where hazardous fine particles are present and where respiratory protection is essential, such as construction, healthcare, manufacturing, mining, laboratories, and firefighting, could benefit from this technology. All things considered, this database could play a significant role in occupational safety and respiratory health research.

V. CONCLUSION

A database of high-quality IR and RGB videos was created. 62 participants, 36 women and 26 men, each tested 4 FFR in 4 different positions (front, top, left, right) and they performed 2 QNFT for each FFR tested: one before video recording and one after. This database comprises 1054 IR, 1054 RGB videos, and 496 QNFT, totaling 8To. To our knowledge, it currently represents the most comprehensive database in the field of N95 FFR leakage detection using IR imaging.

This database has been specifically created to develop deep learning models for comprehensive N95 FFR leakage detection. These models could automatically locate and quantify leakage across the entire face seal of N95 FFR. This deep learning technology has the potential to provide an alternative to current methods, ensuring adequate respiratory protection for all N95 FFR users, particularly healthcare workers.

DATA ACCESSIBILITY

A website[1] has been developed to showcase a sample database and the procedure to follow in order to obtain it. This database is available only to students, research groups,

[1]https://saferespirator.uqar.ca/

or research institutions with approval from an authorized authority. Therefore, we will not accept applications from generic email addresses (gmail.com, hotmail.com, etc.); only applications from email addresses associated with non-profit institutions such as schools or research institutes will be considered.

This website provides the rules and the license agreement that must be signed and returned. The use of participants' data is clearly outlined in these rules. Any participant who has not signed the consent form to share their face must have their eye area blurred or hidden before their data can be used. A list of each participant's consent status is available on this website and in the database.

Concerning the data, only raw data is provided. The videos are available in.tiff and.ats formats for IR recordings and.mp4 format for RGB videos. For the QNFT results, the Portacount® output is provided as a PDF summarizing the participant number, the N95 FFR model, and the fit factor.

Regarding data organization, the dataset is divided into two collection phases. The first phase includes 35 participants, while the second phase includes 27 participants. For each participant, the data is organized by N95 FFR model. Additionally, for each N95 FFR, the corresponding IR, RGB, and FF data are provided in the previously specified formats, with recordings captured from four different viewpoints: top, left, front, and right.

Additionally, no scripts are included in the dataset. However, an Excel file named *SummaryTable_ToShare* is provided, summarizing participant information such as their number, sex, and facial dimensions (height and width). This file also includes a summary of leakage feeling for each participant and each N95 FFR, numbered 11 to 62, as well as a summary of the QNFT results conducted by the participants.

ACKNOWLEDGMENT

The authors would like to thank all the participants who took part in their data collection. Clemente Ibarra Castanedo and Denis Ouellet for their assistance throughout this study and the individuals working at the 3D printing services at UQAR and ULaval.

REFERENCES

[1] L. A. Pompeii, C. S. Kraft, E. A. Brownsword, M. A. Lane, E. Benavides, J. Rios, and L. J. Radonovich, "Training and fit testing of health care personnel for reusable elastomeric half-mask respirators compared with disposable N95 respirators," *JAMA*, vol. 323, pp. 1849–1852, Mar. 2020.

[2] M. Clayton and N. Vaughan, "Fit for purpose? The role of fit testing in respiratory protection," *Ann. Occupational Hygiene*, vol. 49, no. 7, pp. 545–548, 2005.

[3] S. A. Grinshpun, H. Haruta, R. M. Eninger, T. Reponen, R. T. McKay, and S.-A. Lee, "Performance of an N95 filtering facepiece particulate respirator and a surgical mask during human breathing: Two pathways for particle penetration," *J. Occupational Environ. Hygiene*, vol. 6, no. 10, pp. 593–603, Sep. 2009.

[4] R. J. Roberge, W. D. Monaghan, A. J. Palmiero, R. Shaffer, and M. S. Bergman, "Infrared imaging for leak detection of N95 filtering facepiece respirators: A pilot study," *Amer. J. Ind. Med.*, vol. 54, no. 8, pp. 628–636, Aug. 2011.

[5] *1910.134 App A—Fit Testing Procedures (Mandatory)*. Accessed: Apr. 4, 2024. [Online]. Available: https://www.osha.gov/laws-regs/regulations/standardnumber/1910/1910.134AppA

[6] A. Regli, A. Sommerfield, and B. S. von Ungern-Sternberg, "The role of fit testing N95/FFP2/FFP3 masks: A narrative review," *Anaesthesia*, vol. 76, no. 1, pp. 91–100, Jan. 2021.

[7] Y. J. Huh, H. M. Jeong, J. Lim, H. Y. Park, M. Y. Kim, H. S. Oh, and K. Huh, "Fit characteristics of N95 filtering facepiece respirators and the accuracy of the user seal check among Koreans," *Infection Control Hospital Epidemiology*, vol. 39, no. 1, pp. 104–107, Jan. 2018.

[8] S. C. Lam, J. K. L. Lee, S. Y. Yau, and C. Y. C. Charm, "Sensitivity and specificity of the user-seal-check in determining the fit of N95 respirators," *J. Hospital Infection*, vol. 77, no. 3, pp. 252–256, Mar. 2011.

[9] A. K. Sahu, V. Amrithanand, R. Mathew, P. Aggarwal, J. Nayer, and S. Bhoi, "COVID-19 in health care workers—A systematic review and meta-analysis," *Amer. J. emergency Med.*, vol. 38, no. 9, pp. 1727–1731, 2020.

[10] S. L. Burrer, M. A. de Perio, M. M. Hughes, D. T. Kuhar, S. E. Luckhaupt, C. J. McDaniel, R. M. Porter, B. Silk, M. J. Stuckey, and M. Walters, "Characteristics of health care personnel with COVID-19—United States, February 12-april 9, 2020," *MMWR. Morbidity Mortality Weekly Rep.*, vol. 69, no. 15, pp. 477–481, Apr. 2020.

[11] J. Kerl, M. Wenzel, and D. Köhler, "Thermal imaging of mask leakage during pressure-controlled ventilation (bipap therapy)," *Somnologie*, vol. 8, no. 3, pp. 83–86, 2004.

[12] J. Dowdall, I. Pavlidis, and J. A. Levine, "Thermal image analysis for detecting facemask leakage," in *Thermosense*, vol. 5782. Bellingham, WA, USA: SPIE, 2005, p. 46.

[13] P. Harber, J. Su, A. D. Badilla, R. Rahimian, and K. R. Lansey, "Potential role of infrared imaging for detecting facial seal leaks in filtering facepiece respirator users," *J. Occupational Environ. Hygiene*, vol. 12, no. 6, pp. 369–375, Jun. 2015.

[14] D. Chapman, C. Strong, K. D. Tiver, D. Dharmaprani, E. Jenkins, and A. N. Ganesan, "Infra-red imaging to detect respirator leak in healthcare workers during fit-testing clinic," *IEEE Open J. Eng. Med. Biol.*, vol. 5, pp. 198–204, 2024.

[15] C. R. Siah, S. T. Lau, S. S. Tng, and C. H. M. Chua, "Using infrared imaging and deep learning in fit-checking of respiratory protective devices among healthcare professionals," *J. Nursing Scholarship*, vol. 54, no. 3, pp. 345–354, May 2022.

[16] A. Bari, R. Lamoureux-Lévesque, A. Ahmed Si, J. Brousseau, A. Bahloul, B. Clothilde, Y. Yaddaden, and X. Maldague, "COVID-19, wearing N-95 masks in clinical environments: Thermographic detection of air leaks," in *Proc. Int. Conf. Quant. Infr. Thermography*, 2022, pp. 1–10.

[17] Z. Jiang, M. Hu, Z. Gao, L. Fan, R. Dai, Y. Pan, W. Tang, G. Zhai, and Y. Lu, "Detection of respiratory infections using RGB-infrared sensors on portable device," *IEEE Sensors J.*, vol. 20, no. 22, pp. 13674–13681, Nov. 2020.

[18] Google. (2023). *Mediapipe Face*. [Online]. Available: https://developers.googleblog.com/en/mediapipe-enhancing-virtual-humans-to-be-more-realistic/

[19] J. Richter, C. Wiede, S. Kaden, M. Weigert, and G. Hirtz, "Skin temperature measurement based on human skeleton extraction and infrared thermography—An application of sensor fusion methods in the field of physical training," in *Proc. 12th Int. Joint Conf. Comput. Vis., Imag. Comput. Graph. Theory Appl.*, 2017, pp. 59–66.

[20] M. Brenner, N. H. Reyes, T. Susnjak, and A. L. C. Barczak, "RGB-D and thermal sensor fusion: A systematic literature review," *IEEE Access*, vol. 11, pp. 82410–82442, 2023.

[21] C. Chen, B. Yang, S. Song, M. Tian, J. Li, W. Dai, and L. Fang, "Calibrate multiple consumer RGB-D cameras for low-cost and efficient 3D indoor mapping," *Remote Sens.*, vol. 10, no. 2, p. 328, Feb. 2018.

[22] I. R. Spremolla, M. Antunes, D. Aouada, and B. Ottersten, "RGB-D and thermal sensor fusion-application in person tracking," in *Proc. Int. Conf. Comput. Vis. Theory Appl.*, vol. 4, 2016, pp. 610–617.

[23] R. Beschi, X. Feng, S. Melillo, L. Parisi, and L. Postiglione, "Stereo camera system calibration: The need of two sets of parameters," 2021, *arXiv:2101.05725*.

[24] S. Marinetti and P. G. Cesaratto, "Emissivity estimation for accurate quantitative thermography," *NDT & E Int.*, vol. 51, pp. 127–134, Jun. 2012.

[25] K. Rakrueangdet, N. Nunak, T. Suesut, and E. Sritham, "Emissivity measurements of reflective materials using infrared thermography," in *Proc. Int. Multi. Conference Engineers Comput. Scientists (IMECS)*, 2016, pp. 1–12.

[26] Q. Gu, K. Herakleous, and C. Poullis, "3DUNDERWORLD-SLS: An open-source structured-light scanning system for rapid geometry acquisition," 2014, *arXiv:1406.6595*.

[27] G. Yuan, N. A. Drost, and R. A. McIvor, "Respiratory rate and breathing pattern," *McMaster Univ. Med. J.*, vol. 10, no. 1, pp. 23–25, 2013.
[28] Z. Zhuang, B. Bradtmiller, and R. E. Shaffer, "New respirator fit test panels representing the current us civilian work force," *J. Occupational Environ. Hygiene*, vol. 4, no. 9, pp. 647–659, 2007.
[29] *OBStudio Software*. Accessed: May 22, 2024. [Online]. Available: https://obsproject.com/
[30] FLIR Syst. Inc. *ResearchIR Max Software*. Accessed: May 20, 2024. [Online]. Available: https://www.flir.eu/products/flir-research-studio?vertical=rd+science&segment=solutions
[31] (2024). *Manuel D'utilisation PortaCount Pro 8030/8038*. [Online]. Available: https://tsi.com/getmedia/c8670f72-bd42-4281-9dac-42b09690adb2/8030-8038_PortaCountPro-Manual-FR-6001873?ext=.pdf
[32] M. Arbane, G. Marchais, B. Topilko, Y. Yaddaden, J. Brousseau, X. Maldague, C. Brochot, and A. Bahloul, "Enhanced face mask segmentation on infrared images using lightweight u-net techniques," in *Proc. IEEE Int. Multi-Conference Smart Syst. Green Process-2024*, Apr. 2024, pp. 1–14.
[33] S. Chandaka, A. Chatterjee, and S. Munshi, "Cross-correlation aided support vector machine classifier for classification of EEG signals," *Expert Syst. Appl.*, vol. 36, no. 2, pp. 1329–1336, Mar. 2009.
[34] L. B. White and B. Boashash, "Cross spectral analysis of nonstationary processes," *IEEE Trans. Inf. Theory*, vol. 36, no. 4, pp. 830–835, Jul. 1990.
[35] P. Sedgwick, "Pearson's correlation coefficient," *Bmj*, vol. 345, pp. 1–26, Apr. 2012.

GEOFFREY MARCHAIS received the Master of Engineering (M.Eng.) degree from the École Nationale Supérieure d'Arts et Métiers (ENSAM) and the Master of Science degree (M.Sc.A) in applied sciences from the Université du Québec Ã Rimouski (UQAR), Québec City, Canada. He is currently pursuing the Ph.D. degree with the École de Technologie Supérieure (ETS), Montreal, specializing in the dynamic study of vibrations in suspension seats. His research interests include collaborations with various institutions and experts in mechanical and biomedical engineering.

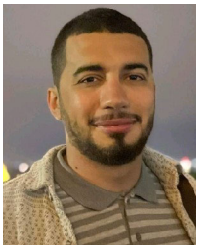

MOHAMED ARBANE (Graduate Student Member, IEEE) received the B.S. degree in electronics from the University of M'sila, Algeria, in 2019, and the master's degree in embedded systems in Algeria. He is currently pursuing the master's degree in engineering with UQAR/Laval, Canada. His research interests include artificial intelligence, deep learning, computer vision, natural language processing, data science, and infrared technology.

BARTHELEMY TOPILKO received the M.S. degree in engineering from the Université du Québec Ã Rimouski and the Engineering Diploma degree from the Ecole Nationale Supérieure d'Arts et Métiers, in 2024. Since September 2024, he has been a Thermal Engineer with the start-up NAAREA. He is the author of two conference papers (LATAM SHM 2023 and IEEE UBMK 2024). His research interests include CFD and thermal finite element computation and infrared imaging technologies.

JEAN BROUSSEAU received the Ph.D. degree in mechanical engineering from Laval University, Québec City. He is currently a retired Professor with the Université du Québec Ã Rimouski, where he is actively engaged in research as an Associate Professor. He held the NSERC-UQAR Research Chair in design engineering, until 2023. His research interests include mechanical system design, material behavior, finite element modeling and simulation, and industrial applications of 3D metal printing. He is also a member of the Ordre des Ingénieurs du Québec.

CLOTHILDE BROCHOT received the M.S. degree in physics from the University of Lyon 1, France, in 2008, and the Ph.D. degree in process engineering from the University of Lorraine, France, in 2012. She is currently an IRSST Research Professional and an Associate Professor with ÉTS and UQAR. Between 2013 and 2021, she was with IRSST and Concordia University (a Postdoctoral Fellow and a Research Associate) setting up and managing a particle filtration research laboratory. She has worked for both research institutes and companies, mainly in the field of respiratory protection equipment. Her research interests include the protection of workers exposed to airborne contaminants in their working environment, particularly from the point of view of aerosol physics and filtration mechanics.

YACINE YADDADEN received the bachelor's and master's degrees in electrical engineering, with a focus on intelligent and communicating systems from the Université des Sciences et de la Technologie de Houari Boumediene, Algeria, where he is currently pursuing the Doctorate degree in information science and technology in telecommunications. At the same time, he worked for a company specializing in internet access and services. In 2015, he joined the Université du Québec Ã Chicoutimi to pursue the Ph.D. degree, focusing his work on artificial intelligence. After completing the Ph.D. degree, he had the opportunity to complete a postdoctoral fellowship with Université Laval, while lecturing in computer science with the Université du Québec Ã Rimouski and Cégep de Limoilou. In July 2020, he joined as a Faculty Member of the Université du Québec Ã Rimouski, specializing in computer vision and machine learning.

ALI BAHLOUL has been a Researcher with IRSST, since 2005, has developed expertise in the field of industrial ventilation and indoor air quality. He is currently an Associate Professor with the Montréal's École de Technologie Supérieure and Concordia University and an Adjunct Professor with the Université de Montréal. His research interests include anticipate, identify, evaluate, and control exposure to chemical substances and biological agents. His work focuses on developing and validating methods for revaluating ventilation efficiency, studying ventilation system components and aeraulic parameters of emission, and developing and validating source capture devices. He also works on developing and using analytical methods. In addition, he has expertise in hydrodynamic instability, dual diffusion, and heat and mass transfers.

XAVIER MALDAGUE (Life Senior Member, IEEE) received the B.Sc., M.Sc., and Ph.D. degrees in electrical engineering from Université Laval, Québec City, QC, Canada, in 1982, 1984, and 1989, respectively. He has been a Full Professor with the Department of Electrical and Computing Engineering, Université Laval, since 1989, where he was the Head of the Department, in 2003, 2008, 2018, 2023, 2024, and 2025. He has trained over 50 graduate students (M.Sc. and Ph.D.) and has more than 300 publications. His research interests include infrared thermography, nondestructive evaluation (NDE) techniques, and vision/digital systems for industrial inspection. He is a Honorary Fellow of Indian Society of Nondestructive Testing. He is also a fellow of Engineering Institute of Canada Canadian Engineering Institute, the American Society of Nondestructive Testing, and the Alexander von Humbolt Foundation, Germany. He holds the Tier 1 Canada Research Chair in Infrared Vision. In 2019, he was bestowed an Doctor Honoris Causa in Infrared Thermography by University of Antwerp, Belgium.